On the relationship between wind observation accuracy and the ascending node of sun-synchronous orbit for the Aeolus-type spaceborne Doppler wind lidar

Chuanliang Zhang[1,2], Xuejin Sun[2], Wen Lu[2], Yingni Shi[1], Naiying Dou[1], and Shaohui Li[1,2]

[1]Mailbox 5111, Beijing 100094, China

[2]College of Meteorology and Oceanography, National University of Defense Technology, Nanjing 211101, China

Corresponding to: Xuejin Sun (xuejin.sun@outlook.com)

Abstract. The launch and operation of first spaceborne Doppler wind lidar (DWL) Aeolus is of great significance in observing global wind field. Aeolus operates on the sun-synchronous dawn-dusk orbit to minimize the negative impact of solar background radiation (SBR) on wind observation accuracy. For that the future spaceborne DWLs may not operate on sun-synchronous dawn-dusk orbits due to their observation purposes, the impact of the local time of ascending node (LTAN) crossing of sun-synchronous orbits on the wind observation accuracy was studied in this paper by proposing two added Aeolus-type spaceborne DWLs operated on the sun-synchronous orbits with LTANs of 15:00 and 12:00. On the two new orbits, the increments of averaged SBR received by the new spaceborne DWLs range from 39 to 56 $mW \cdot m^{-2} \cdot sr^{-1} \cdot nm^{-1}$ under cloud-free skies near summer and winter solstices, which will lead to the increment of averaged Rayleigh channel wind observation uncertainties of 0.19 m/s for 15:00 orbit and 0.27 m/s for 12:00 orbit when the instrument parameters of new spaceborne DWLs are the same with those of Aeolus with 30 measurements per observation with 20 laser pulses per measurement. Increasing laser pulse energy of the new spaceborne DWLs is used to lower the wind observation uncertainties. Furthermore, a method to quantitatively design the laser pulse energy according to specific accuracy requirements is given in this paper based on the relationship between the signal noise ratio and the uncertainty of response function of Rayleigh channel. The laser pulse energies of the two new spaceborne DWLs are set to 70 mJ based on the statistical results according to the method, meanwhile other instrument parameters are the same as those of Aeolus. Based on the parameter proposal, the accuracy of about 77.19% and 74.71% of the bins of two new spaceborne DWLs would meet the accuracy requirements of European Space Agency (ESA) for Aeolus, of which values are closely equivalent to the percentage of 76.46% when Aeolus are free of the impact of SBR. And the averaged uncertainties of the two new spaceborne DWLs in free troposphere and stratosphere are 2.62 and 2.69 m/s respectively, which perform better than that of Aeolus (2.77 m/s).

1 Introduction

The first spaceborne Doppler wind lidar (DWL) mission ADM-Aeolus (ADM, Atmospheric Dynamics Mission) designed by European Space Agency (ESA) was launched successfully on 22 August 2018, which improves people's knowledge on global wind field. Aeolus carries a spaceborne DWL, Atmospheric Laser Doppler Instrument (ALADIN), has been used to make

preliminary observations of global wind field since the launch. And the first Numerical Weather Prediction (NWP) experiments show that the assimilated wind observations have significant positive impact on the forecast of wind, humidity and temperature at short-range, especially in the tropical troposphere and south hemisphere (Straume *et al.*, 2019). Furthermore, scientists have also designed several possible observation scenarios of future spaceborne DWLs. Considering Aeolus can only realize the observations of single horizontal line-of-sight (LOS) wind components, Ma *et al.*, (2015) and Masutani *et al.*, (2010) proposed a spaceborne DWL concept with two pairs of telescopes (azimuth angles from one pair is 45° and 315°, the other pair is 135° and 225°) using both coherent-detection and direct-detection technology, and ISHII *et al.*, (2017) proposed the spaceborne coherent DWL concept with one pair of telescopes (azimuth angles of 45° and 315°), both of the two observation scenarios can provide the horizontal vector wind. In addition, Marseille et al. (2008) demonstrated that larger observation coverage is more beneficial in the improvement of NWP results in global scale compared to the measurement of horizontal vector wind by proposing several multi-satellites joint observation scenarios with Aeolus-type instruments. However, the measurements of horizontal vector wind perform better for NWP results in the region close to the satellite tracks. In short, Aeolus is a demonstration mission which primarily aims to improve NWP and medium-range weather forecast, and there will be more observation scenarios of spaceborne DWLs with different observation purposes launched in the future.

Aeolus operates on the sun-synchronous, dawn-dusk orbit to minimize the impact of solar background radiation (SBR) on the accuracy of wind observations (Heliere *et al.*, 2002, Baars *et al.*, 2019). The SBR is defined as the top-of-atmosphere (TOA) radiance which directs to the telescopes of spaceborne DWLs, and the solar background noise (SBN) is the photon counts excited by SBR and imaged on the photon detectors (Zhang *et al.*, 2018) which would lower the observation accuracy by Poisson noise (Liu *et al.*, 2006, Hasinoff *et al.*, 2010). The dawn-dusk orbit is an optimal proposal to lower SBR for spaceborne DWLs operating on sun-synchronous orbits. The future spaceborne DWLs may operate on different orbits which should be related to their observation purposes. For example, according to Marseille et al. (2008), larger coverage of wind observations would perform better in improving results of NWP. Furthermore, if the wind field at about 00:00/12:00 or 03:00/15:00 can be observed, we can reconstruct the wind speed diurnal cycle combing with the wind observations of Aeolus. If the future spaceborne DWLs would operate on the sun-synchronous orbits with different local time of ascending node (LTAN) crossing, the received SBR would become larger which would lead to higher uncertainties of wind observations.

According to the technology mechanism of Aeolus, the factors that affect the observations accuracy of spaceborne DWLs include atmospheric heterogeneity, SBR, et al. Aeolus is a direct-detection Doppler wind lidar which senses winds through Mie channel and Rayleigh channel. Mie channel senses winds using the laser signal backscattered from aerosol/cloud particles, and Rayleigh channel sensing winds using molecular backscatter signal. Atmospheric heterogeneity mainly affects the wind observations on Mie channel. Sun *et al.*, (2014) indicate that typical values for wind uncertainties on Mie channel in the free troposphere are in the range of 1~1.5 m/s caused by atmospheric heterogeneity, which cannot be easily corrected. And for Rayleigh channel, the uncertainties caused by atmospheric heterogeneity range between 0.2 and 0.6 m/s in the troposphere,

which can be largely reduced by scene classification algorithm. SBR mainly affects the observations on Rayleigh channel, and has less impact on the observations in Mie channel (Rennie, 2017). The study of Zhang *et al.*, (2019) illustrates that the received SBR of Aeolus ranges from 0 to 169 $mW \cdot m^{-2} \cdot sr^{-1} \cdot nm^{-1}$. And when the SBR is greater than 80 $mW \cdot m^{-2} \cdot sr^{-1} \cdot nm^{-1}$, the whole profiles of wind observations would be less accurate.

The observations of global wind would improve the results of NWP, however, if the observations of low accuracy are assimilated, the negative impact on NWP results would be introduced (Stoffelen *et al.*, 2005, 2006). According to the accuracy requirements of ESA, the uncertainties of the horizontally projected line-of-sight (HLOS) wind observations in the Planetary Boundary Layer (PBL), free troposphere, and stratosphere should be less than 1, 2, and 3 m/s respectively (Stoffelen et al., 2005). And the latest research also demonstrated that the uncertainties of 1 m/s in PBL, 2.5 m/s in free troposphere, and 3~5 m/s in stratosphere would also allow significant positive impact in NWP results (Straume *et al.*, 2019). The height boundary between the PBL, free troposphere and stratosphere are 2 km and 16 km respectively. In this paper, we assumed that the accuracy of 5 m/s in stratosphere was required. The troposphere mentioned below specially referred to the free troposphere.

Assuming the future Aeolus-type spaceborne DWLs will operate on the sun-synchronous orbits with different LTANs, the distributions of received SBR near winter and summer solstices and corresponding uncertainties of wind observations caused by SBR were figured out in this paper. The method to lower the uncertainty to specific accuracy level, i.e. to meet the accuracy requirements of ESA, or to reach the similar accuracy level of Aeolus, was also discussed. In general, the only way to reduce the effect of Poisson noise was to capture more signal (Vahlbruch *et al.*, 2008). According to the lidar equation, the following methods can be used to increase return signal energy of spaceborne DWLs: 1) increasing the laser pulse energy; 2) lowering the height of orbits; 3) enlarging the telescope aperture; 4) reducing vertical resolution (Marseille and Stoffelen, 2003). In addition, the orbit height of Aeolus was adjusted from originally designed 400 km to 320 km to increase energy of received signal. In this paper, increasing laser pulse energy was used to lower the uncertainty. The remainder of this paper is organized as follows. The details of the orbits of the three spaceborne DWLs and the Aeolus-type spaceborne DWL simulation system are presented in Sect. 2. Section 3 gives a method to quantitatively design the laser pulse energy of spaceborne DWLs based on specific accuracy requirements. Before that, the relationship between the signal noise ratio (SNR) and the uncertainty of response function of Rayleigh channel is also discussed. In Sect. 4, the preliminary proposal of laser pulse energy of the two new spaceborne DWLs is given using the method mentioned in Sect. 3 based on the global distributions of SBR and wind observation uncertainties, as well as the accuracy requirements for spaceborne DWLs. Sect. 5 presents the summary and conclusions.

2 The sun-synchronous orbits and simulation system of spaceborne DWLs

In general, for sun-synchronous orbits, the spaceborne DWL running on the dawn-dusk orbit (LTAN of 18:00) would receive minimum SBR, and the spaceborne DWL running on the noon-midnight orbit (LTAN of 12:00) would receive maximum SBR. In order to study the impact of orbit selection on the wind observation accuracy, the spaceborne DWLs operating on three sun-synchronous orbits with LTANs of 18:00, 15:00, and 12:00 respectively were proposed. And the simulation system used to calculate the uncertainty of wind observations was also described.

2.1 The sun-synchronous orbits

The three sun-synchronous orbits with LTANs of 18:00, 15:00, and 12:00 are illustrated in Fig.1 (a). Aeolus operating on the sun-synchronous, dawn-dusk orbit with height of 320 km is marked in blue. The spaceborne DWL is equipped with a single-perspective telescope, which scanning at 90° with respect to the satellite track, under a slant angle of 35° versus nadir, measuring profiles of HLOS wind components. The other two spaceborne DWLs running on the sun-synchronous orbit with LTANs of 15:00 and 12:00 which are marked in yellow and red lines respectively. The intersection points between laser beam and earth surface are called off-nadir points of which lines are illustrate in Fig. 1(b).

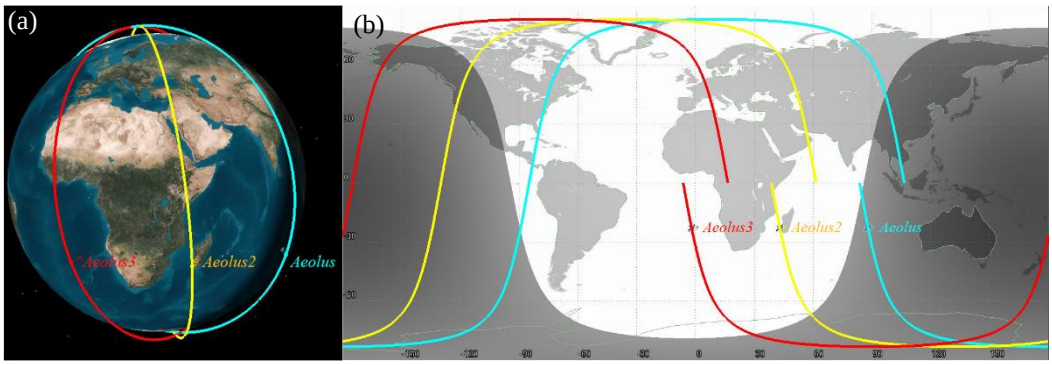

Figure 1. The orbits of the spaceborne DWLs operating on the sun-synchronous orbits with LTAN of 18:00, 15:00, and 12:00, which are marked in blue, yellow, and red respectively. (a) 3D graphics; (b) 2D graphics.

The two new spaceborne DWLs are assumed to be Aeolus-type instruments whose instrument parameters the same as those of Aeolus except different laser pulse energies which aims to improve wind observation accuracy. When demonstrating the instrument parameters of spaceborne DWLs, people also pay attention to the observation accuracy under worst cases. Solar zenith angle is the dominant factor for SBR received by spaceborne DWL. The variations of solar zenith angles of the off-nadir points on the three orbits within one-year range are illustrated in Fig. 2, which indicates that received SBR would reach maximum values near summer solstice and reach maximal values near winter solstice. For the off-nadir points in the north hemisphere, SBR will reach maximum near summer solstice. And SBR will reach maximum near winter solstice for the off-nadir points in the south hemisphere. In this paper, the global distributions of maximum SBR in 1°×1° grid near the summer solstice which range from June 14 to 28 and near the winter solstice which ranges from December 15 to 30 are used for the investigations of the worst cases with maximum Rayleigh channel wind observation uncertainties due to SBR. Furthermore,

the annual variation characteristics of solar zenith angles are less obvious on the two new orbits compared to that of Aeolus as shown in Fig. 2, which indicates that the observations of two new spaceborne DWLs would more likely to suffer worst cases on Rayleigh channel compared to that of Aeolus.

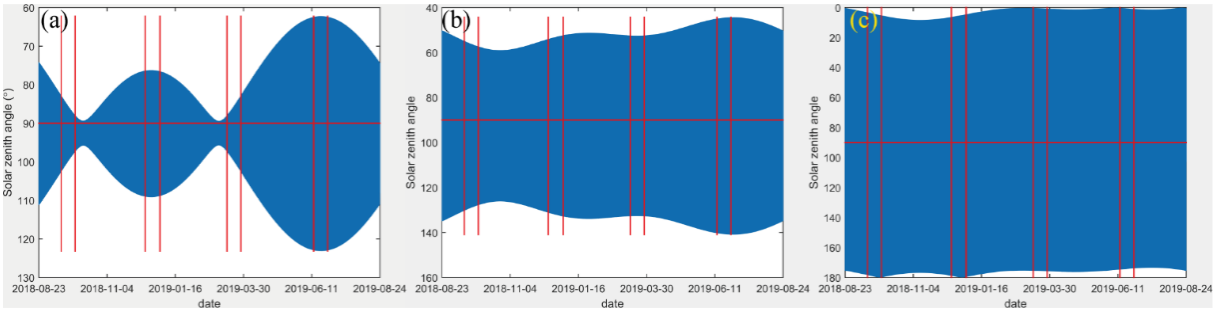

Figure 2. The variations of solar zenith angles of the off-nadir points on the three orbits within one-year range. The 4 time ranges divided by 8 red lines denote 15 days near autumn equinox, winter solstice, spring equinox and summer solstice respectively. Sun-synchronous orbit with LTANs of 18:00 (a), 15:00(b), and 12:00(c).

2.2 Spaceborne DWL simulation system

An Aeolus-type spaceborne DWL simulation system considering the impact of SBR on wind observation uncertainties was developed to retrieve HLOS wind components and calculate observation uncertainties. The simulation system was built according to the optical structure of Aeolus, which consists of laser transmitter, the telescope and front optics, Mie spectrometer, Rayleigh spectrometer, and detection front units (Marseille and Stoffelen, 2003 and Paffrath, 2006). Considering that SBR mainly affect the observation accuracy of Rayleigh channel, we focused on the simulation of the wind retrieved method on Rayleigh channel, and assumed that the cross-talk effect between Mie channel and Rayleigh channel is negligible. The details of the working principle and instrument parameters of Aeolus used in the simulation system were set according to the ADM-Aeolus Algorithm Theoretical Basis Document (ATBD) Level1B products (Reitebuch *et al.*, 2018), expect laser pulse energy which is set to 60 mJ, which was consist with the laser pulse energy of onboard Aeolus. In addition, in the simulation system, one observation consisted of 30 accumulations (also called as measurements) of 20 shots, resulting in a horizontal averaging length of about 90km per observation. Detection chain noise of 4.7 e^-/pixel on Rayleigh channel for each measurement was also taken into account. The vertical resolutions of retrieved wind were 500 m in the PBL, 1 km in the troposphere, and 2 km in the stratosphere (Marseille et al., 2008).

The input parameters of simulation system included u- and v- components wind, temperature, pressure, aerosol optical properties, and TOA radiance. In this paper, the impacts of SBR on the wind observation accuracy of spaceborne DWLs under cloudy atmosphere were not considered. The first five components were derived from the pseudo-truth global atmospheric condition dataset, which consisted of the Ozone Monitoring Instrument (OMI) database (McPeters *et al.*, 2008), including the latitude-averaged profiles of temperature, pressure, and density of ozone, and the lidar climatology of vertical aerosol structure for spaceborne lidar simulation studies (LIVAS) database (Amiridis *et al.*, 2015), which was used to describe aerosol optical properties. Only aerosols in the PBL were considered here. The details to derive the global distributions of SBR received by

Aeolus-type spaceborne DWLs could refer to Zhang *et al.* (2019), which were briefly introduced here. First, the positions of the off-nadir points of the spaceborne DWLs were obtained using satellite orbit simulation software. Atmospheric conditions were retrieved from the pseudo-truth databases and spatially interpolated to the off-nadir points. The surface albedo was also needed to generate the TOA radiance, which was derived from the database of lambert-equivalent reflectivity (LER) (Koelemeijer *et al.*, 2003). Then the SBR of off-nadir point was generated by radiative transfer model (RTM) libRadtran with the input of atmospheric optical properties, and surface albedo (Emde *et al.*, 2016). Finally, the earth was divided into 1°×1° grid, and the maximum SBR in each grid is picked out as the worst cases of Rayleigh channel wind observation uncertainties due to SBR. Once the atmospheric conditions and SBR were input to the simulation system, the HLOS winds and their corresponding uncertainties in the grids could be figured out.

3 Methodology

Method of increasing the laser pulse energies of Aeolus-type spaceborne DWLs was used to lower wind observation uncertainties in this paper. To assess the performance of spaceborne DWLs under worst cases of Rayleigh channel, and quantitatively design the laser pulse energies of two new spaceborne DWLs as mentioned in Sect. 2.1, the steps are as follows: 1) the global distributions of maximum SBR received by the spaceborne DWLs on the three orbits were figured out to compare the SBR received by the two new spaceborne DWLs with that of Aeolus; 2) the uncertainties of wind observations on Rayleigh channel of the three spaceborne DWLs were derived and the uncertainty increments of the two new spaceborne DWLs compared to that of Aeolus were figured out; 3) the relationship between wind observation uncertainty and laser pulse energy was established; 4) the values of laser pulse energies which would lower the uncertainties to required accuracy level were derived based on the relationship established in the step 3).

3.1 Uncertainty of wind observation on Rayleigh channel

The double-edge technique is used to retrieve the HLOS wind components on Rayleigh channel for Aeolus (Flesia and Korb, 1999, Zhang et al., 2014). The study of Tan *et al.*, (2008) shows that the uncertainty on Rayleigh channel is determined by response function, temperature, and pressure. Lookup table between wind speed and response function, temperature, pressure is established prior to the launch of Aeolus. In operation mode, the profiles of temperature and pressure are obtained from the European Centre for Medium-Range Weather Forecasts (ECMWF) data assimilation system. Once the response function of Rayleigh channel is detected by spaceborne DWL, wind speed will be figured out. The uncertainty of wind observation is estimated as

$$\sigma_{v_{HLOS}} = \frac{\partial v_{HLOS}}{\partial R_{ATM}} \sigma_{R_{ATM}} \quad (1)$$

where $\sigma\cdot$ denotes uncertainty, $\partial\cdot$ denotes partial derivative. v_{HLOS} means the HLOS wind component. R_{ATM} means response function of Rayleigh channel which is defined as

$$R_{ATM} = \frac{N_A - N_B}{N_A + N_B} \quad (2)$$

where N_A and N_B are the useful signal detected by Rayleigh channel.

The $\partial v_{HLOS}/\partial R_{ATM}$ is a function of temperature and pressure, which ranges from 420 to 520 m/s upon most occasions, as shown in Fig. 1 of Zhang et al., (2019). The uncertainty of response function is derived from

$$\sigma_{R_{ATM}} = \frac{2}{(N_A+N_B)^2}\sqrt{N_B^2\sigma_A^2 + N_A^2\sigma_B^2} \quad (3)$$

where σ_A and σ_B denote the uncertainties of N_A and N_B. Here, N_A and N_B can be obtained using the simulation system of spaceborne DWLs. Taking the SBR and noise of spaceborne DWL detectors into account, according to the feature of Poisson noise, the uncertainties in N_A and N_B can be estimated as

$$\sigma_A^2 = N_A + N_{S,A} + N_{noise}^2, \sigma_B^2 = N_B + N_{S,B} + N_{noise}^2 \quad (4)$$

where the $N_{S,A}$ and $N_{S,B}$ are the photon counts which are excited by SBR on Rayleigh channel. N_{noise} denote the noise of detection unit on Rayleigh channel.

$N_{S,A}$ and $N_{S,B}$ can be derived using the following method: the SBR is viewed as the spectrum following the uniform distribution, of which energy can be obtained using Eq. (5) (Nakajima *et al.*, 1999), and the bandwidth equals to that of the interference filter of the Rayleigh channel. $N_{S,A}$ and $N_{S,B}$ can be obtained from the simulation system with the input of the spectrum.

$$S_{SBR} = nE_Q E_O L_S \varphi_R \frac{A_r^2\cdot\pi}{4}\Delta\lambda\Delta t \quad (5)$$

where S_{SBR} denotes the energy of SBR, n denotes the number of the accumulated laser shots, E_Q and E_O denote the quantum efficiency of the detector on Rayleigh channel (Reitebuch *et al.*, 2018), L_S denotes the TOA radiance of the off-nadir point. As to the instrument parameters, φ_R denotes the field of view; A_r denotes the diameter of the telescope; $\Delta\lambda$ denotes the bandwidth of the interference filter. Δt denotes the laser detection time which was dependent on the vertical resolution.

3.2 Relationship between uncertainty and laser pulse energy

The laser pulse energy of laser transmitter has an important influence on the uncertainty of wind observation. Provided that the atmospheric conditions remain unchanged, the higher the laser energy, the backscattered signal received by the telescope of Aeolus-type instrument will become stronger, and the influence of corresponding Poisson noise will be smaller, which will lower the uncertainty of wind observation finally. However, the quantitative relationship between laser pulse energy and wind observation uncertainty is not yet derived due to the fact that the wind observation uncertainties are affected by various factors such as the atmospheric conditions and instrument parameters. In this paper, the method for quantitative derivation of the laser

pulse energy according to specific accuracy requirement of wind observation is proposed through establishing the relationship between SNR of Rayleigh channel and uncertainty of response function of Rayleigh channel.

According to the characteristics of Poisson noise, Marseille and Stoffelen, (2003) defined the SNR of Rayleigh channel.

$$SNR_{Ray} = \frac{N_A+N_B}{\sqrt{N_A+N_B+N_{S,A}+N_{S,B}+2N_{noise}^2}} \tag{6}$$

For the Rayleigh channel of spaceborne DWL, difference between N_A and N_B is not large, especially when the wind speed is close to zero, $N_A \approx N_B$. Based on the assumption that $N_A \approx N_B$ and $N_{S,A} \approx N_{S,B}$, we derived the relationship between the SNR and uncertainty of response function of the Rayleigh channel.

$$\sigma_{R_{ATM}} \approx \frac{1}{SNR_{Ray}} \tag{7}$$

The details of the derivations and proofs are shown in Appendix. Then the uncertainty of wind observation on Rayleigh channel can be estimated as

$$\sigma_{v_{HLOS}} \approx \frac{\partial v_{HLOS}}{\partial R_{ATM}} \cdot \frac{1}{SNR_{Ray}} \tag{8}$$

While increasing the laser pulse energy, the value of $N_A + N_B$ will proportional increase; similarly, $N_{S,A} + N_{S,B}$ will proportional increase with the increase of SBR, which can be written as

$$E_{laser} \propto N_A + N_B, S_{SBR} \propto N_{S,A} + N_{S,B} \tag{9}$$

According to Eqs. (6) and (8), setting $x = N_A + N_B$, which is in proportion to the energy of laser pulse E_{lasr}; $y = N_{S,A} + N_{S,B}$, which is in proportion to the energy of SBR S_{SBR}, and $z = \sigma_{HLOS}$, $f(T,P) = \partial v_{HLOS}/\partial R_{ATM}$, $C = 2N_{noise}^2$, where T denotes temperature and P denotes pressure, the relationship between x, y, and z can be expressed as

$$z \approx f(T,P)\frac{\sqrt{x+y+C}}{x} \tag{10}$$

Equation (10) can be solved as

$$x \approx \frac{f^2(T,P)+f(T,P)\cdot\sqrt{f^2(T,P)+4z^2(y+C)}}{2z^2} \tag{11}$$

Equation (10) illustrates that the uncertainty is determined by temperature, pressure, variable x, the SBR, and dark noise of the detector. The value of x can be estimated using Eq. (11). Knowing the value of x, the value of laser energy cannot be figured out for that the variable x is dependent on the laser energy and wind speed. However, when the wind speed keeps unchanged, the variable x would be in proportion to the energy of laser pulse E_{laser}. That is to say, if the laser energy increases by several times, the corresponding value of variable x will increase by the same multiples when the HLOS wind speed keeps unchanged. Then the required value of laser energy can be obtained based on the proportional relationship between x and E_{laser}.

3.3 Derivation of laser pulse energy

In Sect. 3.2 and Appendix, the relationship between laser pulse energy E_{laser} and wind observation uncertainty was established based on some assumption and simplifications. The following method was used to solve the problem that how much the laser energy could be set to increase the accuracy of the observation of new spaceborne DWLs to the meet specific accuracy requirements.

Firstly, the laser pulse energies of the two new spaceborne DWLs were assumed to be 60 mJ of which parameters are the same as those of Aeolus, the profiles of uncertainties were derived using simulation system based on the global distributions of maximum SBR on the three orbits; secondly, the profiles of variable x at each bin (layer, the concept can refer to Fig. 5 in Tan et al., (2008)) were figured out using Eq. (11), which were set as $x1$. Provided that the accuracy requirements of the two new spaceborne DWLs are to reach the accuracy level of Aeolus, then, the uncertainties of the new spaceborne DWLs were replaced with the uncertainties of Aeolus at the same bins, and the variables of $f(T,P)$, y, and C kept unchanged, the variables x were figured out using Eq. (11), which were set as $x2$; finally, according to the proportional relationship between x and laser energy, $E_{new}/E_{Aeolus} \approx x2/x1$, the required laser pulse energy at each bin could be derived. Therefore, we could determine the laser energies of the two new spaceborne DWLs according to the statistical results.

In the same way, if the accuracy requirements of the two new spaceborne DWLs were to meet the accuracy requirements of ESA, we needed to replace the wind observation uncertainties when the laser energy was 60 mJ with the accuracy requirements of ESA when calculating the value of $x2$, and the other steps were the same as above.

4 Results and discussions

The preliminary results to determine the laser pulse energies of two new spaceborne DWLs were presented in this section. To obtain the laser pulse energies, the global distributions of maximum SBR on the three orbits and the corresponding wind observation uncertainties caused by SBR were calculated, firstly. Then the distributions of required laser energies were obtained according to accuracy requirements based on the method mentioned in Subsect. 3.3. Finally, based on the results, the proposal of laser pulse energies of two new spaceborne DWLs was presented. And the global distributions of wind observation uncertainties of the three spaceborne DWLs were figured out according to the instrument parameter proposal. The details were shown in the following subsections.

4.1 Global distributions of maximum SBR on the three orbits

Global distributions of maximum SBR received by the spaceborne DWLs running on the three orbits in summer and winter are shown in Fig. 3 based on the instrument parameters of Aeolus and the three orbits mentioned in Sect. 2.

The contours in Fig. 3 denote the differences between SBR of two new orbits and sun-synchronous dawn-dusk orbit, which demonstrates that the dawn-dusk orbit is an effective solution to minimize received SBR for spaceborne DWL operating

on sun-synchronous orbits. While operating on the sun-synchronous dawn-dusk orbit, the maximum SBR of the off-nadir points located in the southern hemisphere is nearly equal to zero in summer, and the maximum SBR of the off-nadir points located in the northern hemisphere is nearly equal to zero in winter. For the two new orbits, almost the wind observations of few areas are not affected by SBR, which are mainly located in the regions near the Antarctic and Arctic circles. According to the contours, the ascending order of the values of maximum SBR on the three orbits is dawn-dusk orbit, the orbits with LTAN of 15:00, and that of 12:00 respectively. The closer the LTANs of the orbits to noon, the values and the affected area of SBR will become larger. Statistics illustrate that the averaged SBR illustrated in Fig. 3 are 20.99, 60.68, and 76.36 $mW \cdot m^{-2} \cdot sr^{-1} \cdot nm^{-1}$ respectively near the summer and winter solstice periods. The averaged increments of SBR received by new spaceborne DWLs are 60.68-20.99=39.69 $mW \cdot m^{-2} \cdot sr^{-1} \cdot nm^{-1}$ and 76.36-20.99=55.37 $mW \cdot m^{-2} \cdot sr^{-1} \cdot nm^{-1}$ compared to that of Aeolus.

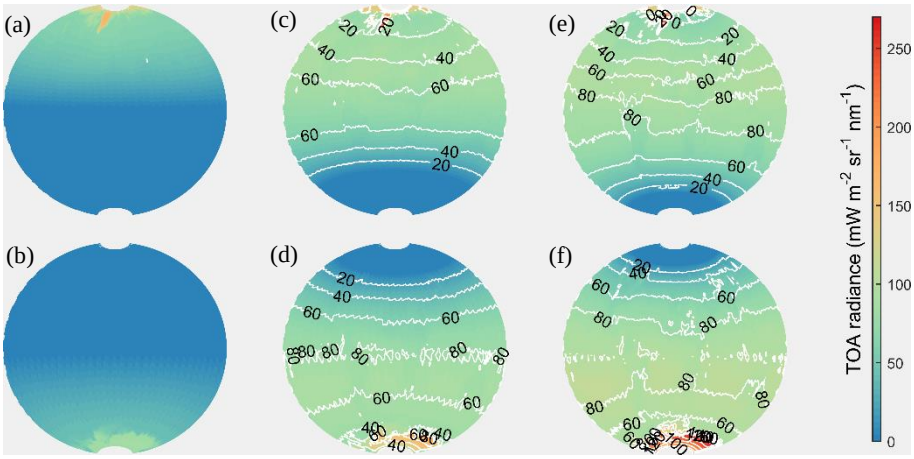

Figure 3. Global distributions of maximum SBR received by spaceborne DWLs operating on the three orbits. Figs. (a, b), (c, d) and (e, f) present the sun-synchronous orbits with LTANs of 18:00, 15:00, and 12:00 respectively, and the upper panels denote the SBR in summer, and the lower panels denote the SBR in winter. The contours in the Figs. (c, e), (d, f) denote the differences between the SBR in Figs. (c, e), (d, f) with the SBR in Figs. (a, b), respectively.

4.2 Uncertainties of wind observations based on the instrument parameters of Aeolus

Figure 3 illustrated the global distributions of maximum SBR near the summer and winter solstice periods, which paid more attention to the worst cases of Rayleigh channel wind observation uncertainties. In fact, for sun-synchronous orbits, nearly half of the off-nadir points would be in darkness which would be free of the impact of SBR, and the other half would be in daylight. As to the off-nadir points in darkness, the global distributions of wind observation uncertainties for Aeolus-type instruments in latitude-averaged were shown in Fig. 4.

Figure 4 illustrates that: 1) Without the impact of SBR, most of wind observations in the free troposphere and stratosphere would meet the accuracy requirements of ESA. The bins of which uncertainties are beyond the requirements of ESA mostly located in the upper layer of troposphere and stratosphere. In addition, the accuracy of wind observations in the PBL is relatively low, which basically cannot meet the requirements of ESA. In fact, the Mie channel is mostly used for wind observations due to the widespread presence of aerosols in PBL. Therefore, the accuracy of the Rayleigh channel in the PBL

is not considered in the following of this paper. Statistics show that the averaged uncertainties without impact of SBR are all about 2.61 m/s in summer and winter, and about 76.46% of the bins would meet the accuracy requirements of ESA overall.

2) Without the impact of SBR, the wind observation uncertainties have little differences among different latitudes.

3) The wind observation uncertainties increase with atmospheric altitudes when the heights of range gates are unchanged. This is mainly due to the fact that molecular number density is proportional to pressure. Near the height of 16 km, the uncertainties decrease first and then increase with the increases in altitude, which attributes to the change in thickness of bins from 1 km to 2 km.

4) Compared with other regions, uncertainties in the equatorial region are higher at the bottom of the troposphere, and lower in the stratosphere. The trend of temperature profile in the equatorial region is the main reason for this phenomenon, which is consist with the trend of uncertainties. Number density of molecules is inversely proportional to temperature. Low molecular number density leads to weak return signal of spaceborne DWLs, which leads to higher wind observation uncertainties.

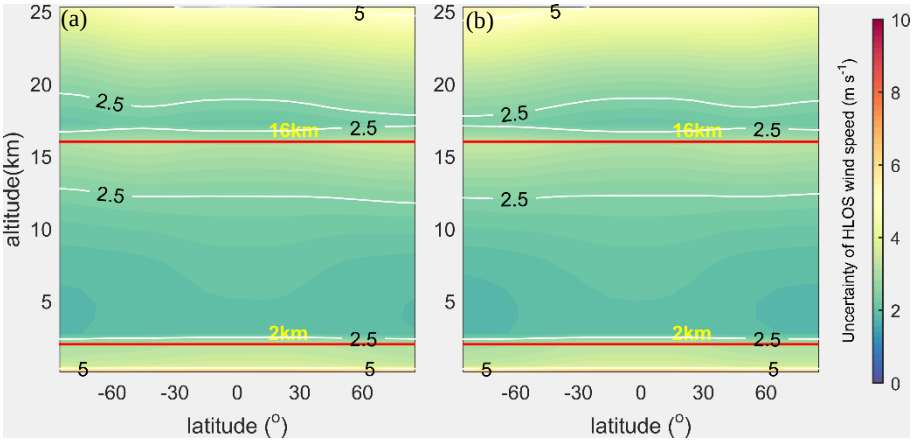

Figure 4. The global distributions of wind observation uncertainties in latitude-average without the impact of SBR. (a) summer; (b) winter.

Based on the global distributions of maximum SBR of the three orbits illustrated in Fig. 3, the worst cases of Rayleigh channel with maximum wind observation uncertainties due to SBR were also derived as shown in Fig. 5. Considering that the distributions of maximum SBR were nearly horizontal to latitudes, and to simplify the calculation, Fig. 5 was obtained using the 10 ° latitude-averaged SBR and atmospheric conditions.

Comparisons between Fig. 4 and Fig. 5 illustrate that wind observation uncertainties become larger with the impact of SBR. And the uncertainties show obvious characteristics of latitudinal variation, which is mainly attributed to the latitudinal variation of maximum SBR shown in Fig. 3. As the LTANs of orbits get closer to noon, the wind observation uncertainties gradually increases, so do the number of bins of which accuracy cannot meet the requirements of ESA. For the bins in the troposphere and stratosphere, about 71.35% can meet the accuracy requirements of ESA for Aeolus, the percentages are 63.45% for the orbit of 15:00 and 60.67% for the orbit of 12:00. The averaged uncertainties of the three spaceborne DWLs in the troposphere and stratosphere are 2.77, 2.96, and 3.04 m/s respectively, which illustrates that the increments in averaged

uncertainties of Rayleigh channel on new orbits are about 3.25-3.06=0.19 m/s and 3.32-3.06=0.27 m/s. Considering that the impact of SBR on the wind observations is minimal on dawn-dusk orbit, and reach maximum on noon-midnight orbit, the phenomenon indicates the selection of the LTANs of sun-synchronous orbits will make the global average wind observation uncertainties a maximum difference of 0.27 m/s for Rayleigh channel of Aeolus-type DWLs near summer and winter solstices. In addition, the global averaged uncertainties without impact of SBR is 2.61 m/s as Fig. 4 indicates, and the global averaged uncertainties is 3.04 m/s under worst cases of Rayleigh channel on the orbit with LTAN of 12:00. The comparison illustrates that SBR caused the maximum increase in the averaged wind observation uncertainty of about 3.04-2.61=0.43 m/s for Aeolus-type DWLs operating on the sun-synchronous orbits.

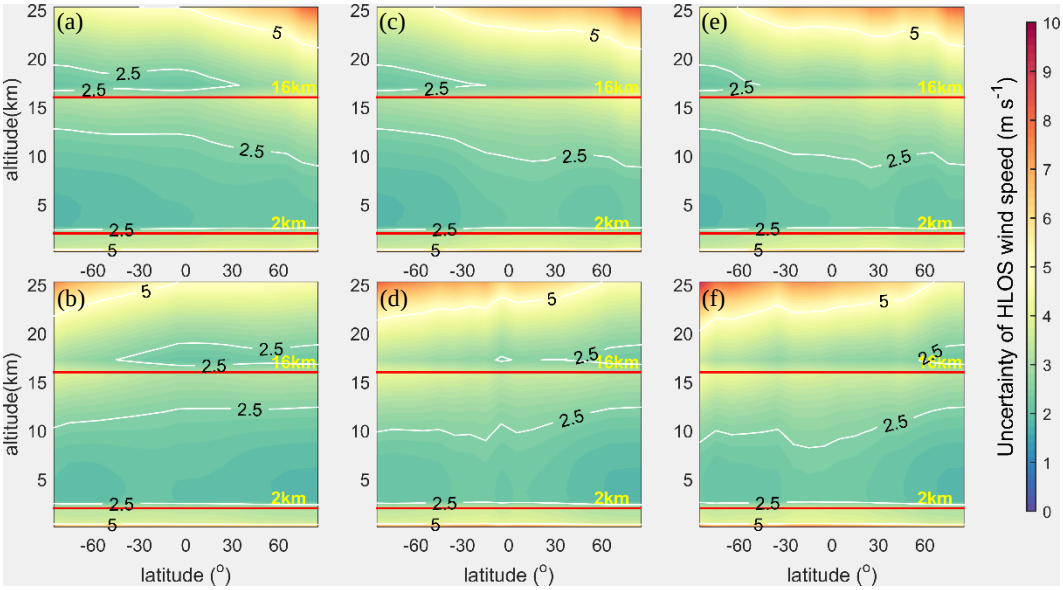

Figure 5. The zonal distributions of Rayleigh channel wind uncertainties in clear air conditions observed by the three spaceborne DWLs operated on the three orbits of which the instrument parameters are the same as those of Aeolus. The contours show the accuracy requirements of ESA. The arrangement of the subgraphs corresponds to that of Fig. 2.

4.3 Distributions of required laser pulse energy

In order to make the accuracy of two new spaceborne DWLs to reach the specific accuracy level under worst cases of Rayleigh channel, the required laser pulse energies were obtained using the method mentioned in Sect. 3.3. According to Eq. (11), the required energy is determined by temperature, pressure, wind uncertainties, SBR, and noise of instrument, thus the required laser pulse energy is different in different bins. Therefore, the laser pulse energies of the new spaceborne DWLs should be determined by the statistics of the profiles of required energy.

Supposed that the wind observation accuracy of the two new spaceborne DWLs is required to reach the accuracy level of Aeolus as shown in Figs. 5(a, b), which can be used for joint observations of the three satellites, the global distributions of required laser pulse energies are derived and illustrated in Fig. 6, which illustrates that for most bins of the two new spaceborne DWLs, it is necessary to increase the laser pulse energy if the accuracy of the wind observation is expected to reach the accuracy level of Aeolus. Especially in the equatorial region, higher laser pulse energy is needed.

Statistics reveal that the averaged values of required laser pulse energies in Fig. 6 is 64.80 mJ for the 15:00 orbit, and 66.59 mJ for the 12:00 orbit respectively. The quantiles of the required energy of the two spaceborne DWLs are shown in Table 1, which means that the corresponding percentages of the bins whose accuracy will reach the accuracy level of Aeolus once the laser pulse energies equal to the specific values. For example, 90% of the bins will reach or exceed the accuracy level of Aeolus when the laser energy is 70.37 mJ for the spaceborne DWL operating on the 15:00 orbit. As we can see from Table 1, when the instrument parameters of two new spaceborne DWLs are the same as Aeolus, of which the laser pulse energies are equal to 60 mJ, only the accuracy of about 20% of the bins can reach the accuracy level of Aeolus near summer and winter solstices. However, as long as the laser energy is slightly increased, the percentages of bins will greatly increase. When the laser pulse energies reach 70 mJ, the accuracy of about 90% of bins could reach or exceed the accuracy level of Aeolus on the orbit 15:00, and the percentage is about 80% on the orbit 12:00.

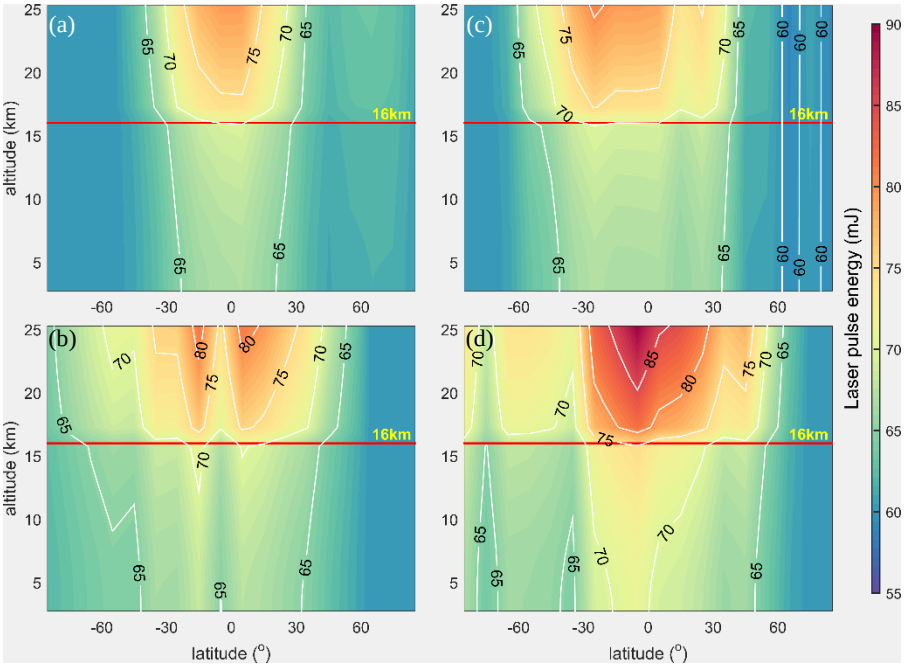

Figure 6. Global distributions of the required laser pulse energies in troposphere and stratosphere to make the wind observation accuracy of two new spaceborne DWLs reach the accuracy level of Aeolus. Figs. 4(a, b) and (c, d) denote the sun-synchronous orbits with LTANs of 15:00 and 12:00 respectively. The upper panels denote the distributions in summer, and the lower panels denote the distributions in winter.

Table 1. Quantiles of the required laser pulse energies of the two new spaceborne DWLs to reach the accuracy level of Aeolus.

Quantile (%)		20	40	50	60	70	80	90	100
Required energy	Orbit 15:00	60.62	62.53	64.00	65.26	66.54	67.85	70.37	81.68
(mJ)	Orbit 12:00	60.71	65.04	66.47	67.34	68.59	70.59	73.74	89.78

Another potential application of the new spaceborne DWLs is to enlarge the global wind observation coverage to improve the forecast results of NWP. It is supposed to have positive impact on NWP results once the wind observation accuracy meets the requirements of ESA. The distributions of required laser pulse energies of the three orbits to meet the accuracy requirements of ESA are illustrated in Fig. 7.

Figure 7 illustrates that the wind observation uncertainties of most bins in the low level of troposphere and stratosphere can meet the accuracy requirements of ESA for the three spaceborne DWLs with the laser pulse energy of 60 mJ. Higher energies are needed in the upper level of troposphere and stratosphere, especially for the regions close to Antarctic and Arctic circles. On the boundary line with height of 16 km, there is an obvious sudden decrease in required laser energies. This is mainly because the vertical thickness of observation bins changes from 1 km in the troposphere to 2 km in the stratosphere, which makes the integration time of detection units of Rayleigh channel double. And larger atmospheric backscattered signal will be integrated. On the other hand, the required wind observation uncertainties increase from 2 m/s to 3 m/s. Therefore, the required laser energies reduce suddenly when going from troposphere to stratosphere near the height of 16 km. Comparisons among the required laser energies of the three orbits illustrate that the closer the orbital LTANs are to noon, the averaged values of the required laser energies will become larger. Statistics show that the averaged values of required energies are 53.27 mJ for Aeolus, 57.60 mJ for the 15:00 orbit, and 59.19 mJ for the 12:00 orbit respectively. The quantiles of the required energies of the three spaceborne DWLs are shown in Table 2. The statistics of Table 2 illustrate that the percentages of bins which can meet the accuracy requirements of ESA increase by 10% even if the laser pulse energy is not increased much when quantile is between 40% to 90%. The averaged increment of laser pulse energy is 6.75 mJ which can increase the quantiles by 10% considering the three orbits as a whole. When the laser pulse energies are set to 67.89, 73.71, and 75.98 mJ, the quantiles will be up to be 80%, which exceeds the percentage of bins (76.46%) for Aeolus without the impact of SBR.

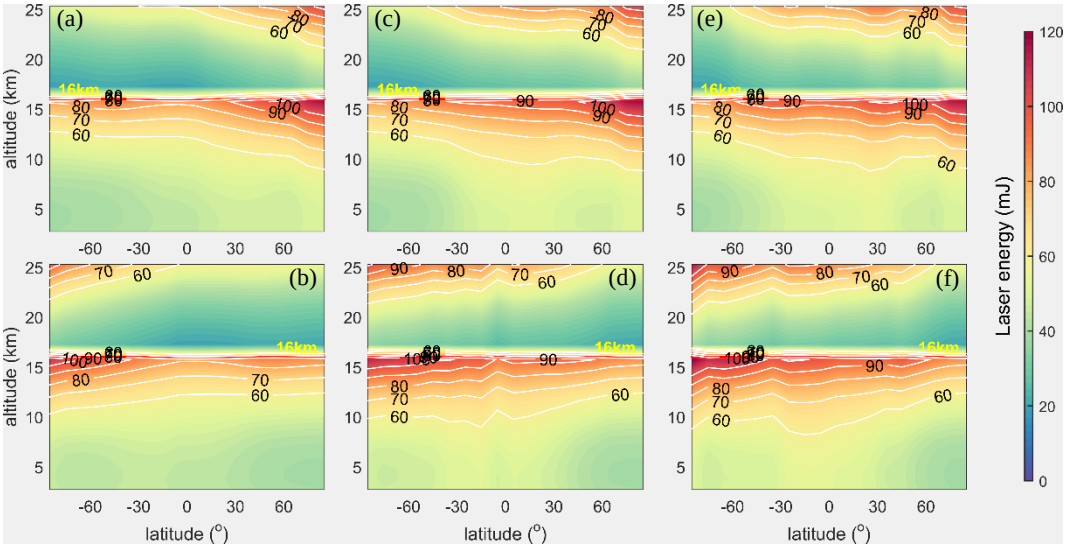

Figure 7. Global distributions of the required laser pulse energies in the troposphere and stratosphere to reach the accuracy requirements of ESA. The arrangement of the subgraphs corresponds to that of Fig. 2.

Table 2. Quantiles of the required laser pulse energy of the three spaceborne DWLs to meet the accuracy requirements of ESA.

Quantile (%)		20	40	50	60	70	80	90	100
Required energy (mJ)	Orbit 18:00	40.93	46.33	49.35	53.87	59.22	67.89	78.63	116.96
	Orbit 15:00	42.83	50.88	53.17	58.21	63.96	73.71	84.88	118.20
	Orbit 12:00	45.06	51.81	54.76	59.86	66.46	75.98	86.82	121.19

4.4 Uncertainties of wind observations resulting from an increased laser pulse energy

In Sect. 4.3, the zonal distributions of required laser pulse energies were derived for different purposes. In order to offer a feasible proposal for the laser pulse energies of the new spaceborne DWLs, the percentages of bins that can meet the specific accuracy requirements when the laser energies reached certain values were figured out, as is shown in Table 3.

Considering the accuracy requirements of ESA and accuracy level of Aeolus, while taking the existing technical level into account, the laser energies of the two new spaceborne DWLs are set to 70 mJ in this paper. In fact, the laser energy of 80 mJ has been already required by ESA in ATBD (Reitebuch *et al.*, 2018). As is shown in Table 3, the percentages of the bins which will meet the accuracy requirements of ESA are 77.19% and 74.71% for orbit 15:00 and 12:00 respectively, close equivalent to the percentage of Aeolus without the impact of SBR (76.46%). In addition, the percentages of the bins are up to 89.04% and 77.34% for orbit 15:00 and 12:00, of which the accuracy of observations equals to or exceeds the accuracy level of Aeolus.

Table 3. Percentages of bins which will meet the specific accuracy requirements with certain laser pulse energies for spaceborne DWLs.

Accuracy requirements		Laser pulse energy (mJ)					
		50	60	70	80	90	100
ESA (%)[a]	Orbit 18:00	51.61	71.35	82.89	90.50	96.64	98.54
	Orbit 15:00	37.13	63.45	77.19	85.53	93.42	97.66
	Orbit 12:00	33.33	60.67	74.71	84.21	91.96	97.22
Aeolus (%)[b]	Orbit 15:00	0	19.44	89.04	99.42	100	100
	Orbit 12:00	0	16.67	77.34	96.78	100	100

[a] The percentage of bins which will meet the accuracy requirements of ESA when the laser energies reach the specific value.

[b] The percentage of bins which will reach the accuracy level of Aeolus in the corresponding bins when the laser energies reach the specific value.

Provided that the three spaceborne DWLs operating on the sun-synchronous orbits shown in Fig. 1, and the instrument parameters of Aeolus keep unchanged. As to the two new Aeolus-type spaceborne DWLs, the other instrument parameters are set as same as those of Aeolus except for the laser pulse energies of 70 mJ. The wind observation uncertainty distributions of the three spaceborne DWLs are derived as is shown in Fig. 8. Note that Figs. 8 (a, b) are identical to those of Figs. 5 (a, b), for that both of them are obtained with laser energies of 60 mJ.

As illustrated in Table 3, when the laser pulse energies of three spaceborne DWLs are 60, 70, and 70 mJ respectively, the percentages of bins which meet the accuracy requirements of ESA are close (71.35%, 77.19%, and 74.71%). And Fig. 8 illustrates that the bins that reach ESA's accuracy requirements are of high consistency in latitude and height distributions. Comparisons among Fig. 8 (c-f) and Fig. 4 illustrate that the wind observation accuracy promotes much in the hemisphere that less affect by SBR. However, limited improvement happens in the other hemisphere. The fact indicates that increasing the

laser energy to 70 mJ cannot compensate the negative influence of large SBR. Comparisons among Fig. 8 (c-f) and Fig. 5 (c-f) show that the wind observation accuracy greatly improved when laser pulse energy increases from 60 mJ to 70 mJ. The fact that such improvements are obtained with only 10 mJ increment in laser pulse energy illustrates that wind observation uncertainties are sensitive to the laser pulse energies of spaceborne DWLs. The averaged uncertainties of the two new spaceborne DWLs with laser pulse energies of 70 mJ in troposphere and stratosphere are 2.62 and 2.69 m/s respectively. Compared to the averaged uncertainties with laser pulse energy of 60 mJ, the difference in uncertainties is 2.96-2.62=0.34 m/s and 3.04-2.69=0.35 m/s, which indicates when the laser pulse energies of two new spaceborne DWLs increase from 60 mJ to 70 mJ, the global averaged wind observation uncertainties will decrease about 0.34 m/s under the impact of maximum SBR.

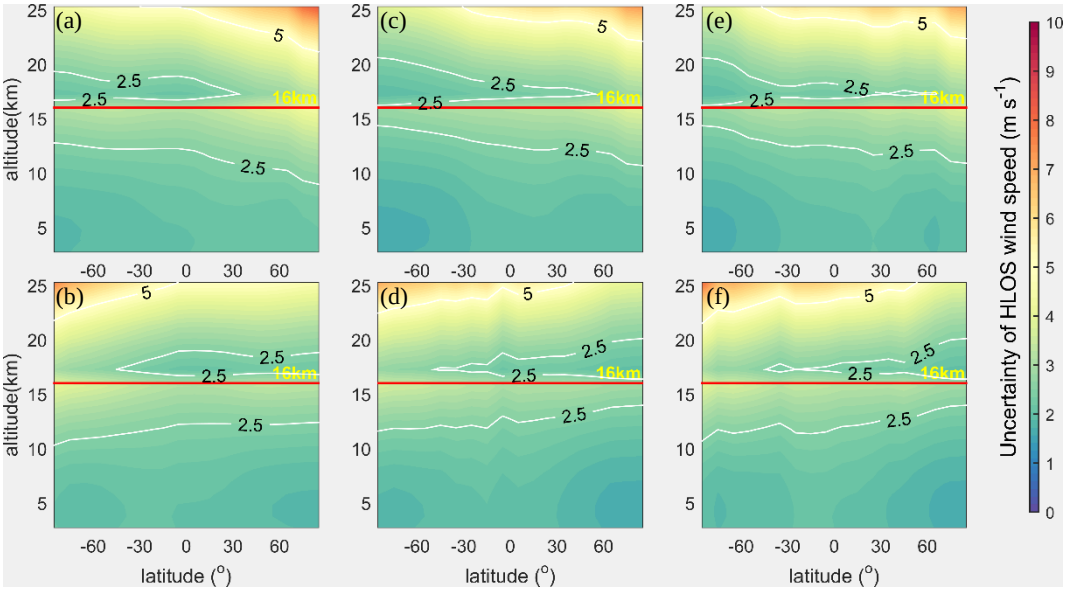

Figure 8. The zonal distributions of wind observation uncertainties of the three spaceborne DWLs with the laser energy of 60 mJ for Aeolus , and with the laser energies of 70 mJ for the two new Aeolus-type spaceborne DWLs. The arrangement of the subgraphs corresponds to that of Fig. 2.

5 Summary and conclusions

The successful launch of Aeolus is significant for people to observe the global wind field. Aeolus operates on the sun-synchronous dawn-dusk orbit to minimize the impact of SBR on the accuracy of wind observations. If the future spaceborne DWLs operate on other sun-synchronous orbits for their specific observation purposes, the received SBR may become larger which would lead to higher observation uncertainties. In general, for sun-synchronous orbits, the spaceborne DWL running on the dawn-dusk orbit (LTAN of 18:00) will receive minimum SBR, and the spaceborne DWL running on the noon-midnight orbit (LTAN of 12:00) will receive maximum SBR. In this paper, the influence of the LTAN crossing of sun-synchronous on the wind observation accuracy for Aeolus-type spaceborne DWLs was studied. And the spaceborne DWL running on three sun-synchronous orbits with LTANs of 18:00, 15:00, and 12:00 respectively were proposed. The method of increasing laser pulse energy of spaceborne DWLs was used to lower the observation uncertainties. Furthermore, the method to quantitatively design laser pulse energy to meet the specific accuracy requirements was also studied.

Assuming two new Aeolus-type spaceborne DWLs operate on the sun-synchronous orbits with LTAN of 15:00 and 12:00. The global distributions of SBR illustrate that the increments of averaged SBR range from 39 to 56 $mW \cdot m^{-2} \cdot sr^{-1} \cdot nm^{-1}$ on the two new orbits near summer and winter solstices compared to that of Aeolus under cloud-free skies, which will lead to the averaged uncertainty increments of 0.19 m/s for 15:00 orbit and 0.27 m/s for 12:00 orbit respectively. Considering that the impact of SBR on the wind observations is minimal on dawn-dusk orbit, and reach maximum on noon-midnight orbit, the phenomenon indicates the selection of the LTAN of sun-synchronous orbits will make the global average wind observation uncertainties a maximum difference of 0.27 m/s for Rayleigh channel of Aeolus-type DWLs near summer and winter solstices. Furthermore, the global averaged uncertainties without impact of SBR is 2.61 m/s, and the global averaged uncertainties is 3.04 m/s under worst cases of Rayleigh channel on the orbit with LTAN of 12:00. The fact illustrates that the maximum increase in the averaged value of global wind observation uncertainty by about 3.04-2.61=0.43 m/s for Aeolus-type DWLs operating on the sun-synchronous orbits due to SBR. In addition, the statistics show that 71.35% of the bins of Aeolus can meet the accuracy requirements of ESA in the free troposphere and stratosphere near summer and winter solstices. For the two new spaceborne DWLs, the percentages are 63.45% for the orbit of 15:00 and 60.67% for the orbit of 12:00. Therefore, it is necessary to increase the laser pulse energies of two new spaceborne DWLs to promote wind observation accuracy and the percentages of bins which could meet accuracy requirements of ESA. On the other hand, wind observation uncertainties are sensitive to laser pulse energy, results in this paper show that the percentages of bins which could meet the accuracy requirements of ESA would increase by 10% with only averaged increment of 6.75 mJ in laser pulse energies considering the three orbits.

To quantitatively design the required laser pulse energies of the new spaceborne DWLs to meet specific accuracy requirements, i.e. to meet the accuracy requirements of ESA, or to reach the similar accuracy level of Aeolus, the relationship between SNR and the uncertainty of response function of Rayleigh channel is established based on some assumption and simplifications, which is proven of wide feasibility by simulation experiments as is shown in Appendix. Finally, the method to derive the required laser energies according to accuracy requirements is proposed.

According to the method, the required energy is determined by temperature, pressure, wind uncertainty, SBR, and noise of instrument, thus the required laser pulse energies are different in different bins. Therefore, the laser pulse energies of the spaceborne DWLs should be determined through the statistics. Considerations are given to both of reaching the accuracy level of Aeolus and improving the forecast results of the NWP, taking existing technical level of spaceborne DWLs into account, the laser pulse energies of two new spaceborne DWLs are set to 70 mJ, while other parameters are the same as those of Aeolus. Based on the parameter proposal, 89.04% and 77.34% of the bins can reach the accuracy level of Aeolus on the two new orbits. And the percentages of bins that meet the ESA's accuracy requirements are 77.19% and 74.71% for the two new spaceborne DWLs, of which values are higher than that of Aeolus (71.35%), and are closely equivalent to the percentage of 76.46% when Aeolus are free of the impact of SBR. The averaged uncertainties of the two new spaceborne DWLs with laser pulse energies

of 70 mJ in free troposphere and stratosphere are 2.62 and 2.69 m/s respectively, which perform better than that of Aeolus (2.77 m/s). Furthermore, when the laser pulse energies of two new spaceborne DWLs increase from 60 mJ to 70 mJ, the global averaged wind observation uncertainties will decrease about 0.34 m/s under the impact of maximum SBR. In summary, it is necessary to increase the laser pulse energies of two new Aeolus-type spaceborne DWLs operating on the sun-synchronous orbits with LTANs of 15:00 and 12:00. The wind measurement accuracy has been greatly improved when laser pulse energies increase from 60 mJ to 70 mJ.

The essence of lowering the wind observation uncertainties of spaceborne DWLs by increasing the laser pulse energies is to increase the SNR of received signal. Other methods can be used to improve the SNR of received signal, such as enlarging the telescope aperture or reducing vertical resolution. Once the quantitative relationship between these instrument parameters and the SNR is established, we can also quantitatively adjust these parameters according to our accuracy requirements as the method shown in this paper.

Appendix

To build the relationship between laser pulse energies and uncertainties of wind observations for Aeolus-type spaceborne DWLs, we derived the relationship between the response function and SNR of Rayleigh channel. According to Eqs. (3) and (4), the uncertainty of response function of Rayleigh channel can be written as follows based on the assumption that $N_A \approx N_B$ and $N_{S,A} \approx N_{S,B}$,

$$\begin{aligned}\sigma_{R_{ATM}} &= \frac{2}{(N_A+N_B)^2}\sqrt{N_B^2\left(N_A+N_{S,A}+N_{noise}^2\right)+N_A^2\left(N_B+N_{S,B}+N_{noise}^2\right)} \\ &\approx \frac{2}{4N_A^2}\sqrt{2N_A^2\left(N_A+N_{S,A}+N_{noise}^2\right)} \\ &= \frac{\sigma_A}{\sqrt{2}N_A}\end{aligned} \tag{A1}$$

According to Eq. (6), the SNR of Rayleigh channel for spaceborne DWLs can be expressed as

$$\begin{aligned}SNR_{Ray} &= \frac{N_A+N_B}{\sqrt{N_A+N_B+N_{S,A}+N_{S,B}+2N_{noise}^2}} \\ &\approx \frac{2N_A}{\sqrt{2\left(N_A+N_{S,A}+N_{noise}^2\right)}} \\ &= \frac{\sqrt{2}N_A}{\sigma_A}\end{aligned} \tag{A2}$$

Therefore,

$$SNR_{Ray} \approx \frac{1}{\sigma_{R_{ATM}}} \tag{A3}$$

As is the equations derivation process shown in Sect. 3.2, the relationship between SNR and uncertainty of response function shown in Eq. (A3) is the basis to derive the relationship between laser pulse energy and wind observation uncertainty shown in Eqs. (10) and (11). However, Eq. (A3) is derived through assumption and simplifications, especially the assumption $N_A \approx N_B$, of which the values may be of large differences when the absolute values of HLOS wind speed are large. To test the

correctness of Eq. (A3) in the actual atmosphere with variable wind speed, we verified the equation using reanalysis data, aerosol optical parameters database LIVAS and surface albedo database. The verification process is shown in Fig. A1.

The reanalysis data is obtained from the 20th Century Reanalysis Project (Compo *et al.*, 2011). In the validation experiment, the monthly averaged 24 level profiles of temperature, pressure, u- and v-component wind with 1°×1° spatial resolution are obtained from the reanalysis data. In this study, the reanalysis data for June 2015 and December 2015 are used as the atmospheric condition in summer and winter respectively. As is shown in Fig. A1, the verification process of Eq. (A3) can be described as follows:

(1) The off-nadir points of spaceborne DWLs are obtained using orbit simulation software based on the orbit information of spaceborne DWLs.

(2) The profiles of temperature, pressure, wind speed, aerosol optical parameters, and surface albedo are interpolated into the off-nadir points.

(3) The SBR of the off-nadir points are derived using RTM libRadtran with the inputs provided in step (2).

(4) The profile values of N_A, N_B and $N_{S,A}$, $N_{S,B}$ are figured out using spaceborne DWL simulation system mentioned in Sect. 2.2 with the inputs of SBR and atmospheric conditions of off-nadir points.

(5) The values of $\sigma_{R_{ATM}}$ and SNR_{Ray} are obtained using Eqs. (3), (4), and (6). In addition, according to ADM-Aeolus ATBD Level1B products (Reitebuch *et al.*, 2018), the noise of detection chain for each measurement is 4.7 e^-/pixel. And 30 measurements are include in one observation, therefore, $C = 2N_{noise}^2 = 2 \times (4.7 \times 30)^2 = 39762$ in Eq. (10) which cannot be negligible.

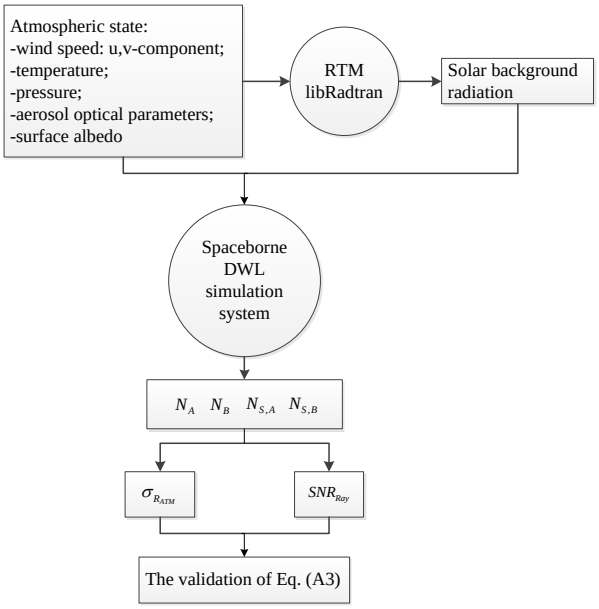

Figure A1. The verification process of Eq. (A3).

The scatters of $\sigma_{R_{ATM}}$ and $1/SNR_{Ray}$ are plotted to verify the accuracy of Eq. (A3), as is shown in Fig. A2. The spatial resolution of the reanalysis data is 1°×1°, so the earth is divided into 1°×1° grid during the verification process, and one off-nadir point in each grid is selected as the verification point. Considering the SBR in summer and winter, and excluding some

grid points with invalid data, a total of 28460 profiles are used in this verification. Each profile contains 24 bins, the verification uses 683040 scattered points.

In the verification, the HLOS wind components derived from u- and v-wind component ranges from -73.02 to 33.14 m/s. Fig. A2 illustrate that the scatter plot between reciprocal SNR and uncertainty of response function of Rayleigh channel is very close to the line $y = x$, which demonstrates that the assumption and simplifications used in deriving the relationship between the laser pulse energy and the uncertainty of wind observation are reasonable, and Eq. (A3) is of wide feasibility in the real atmosphere.

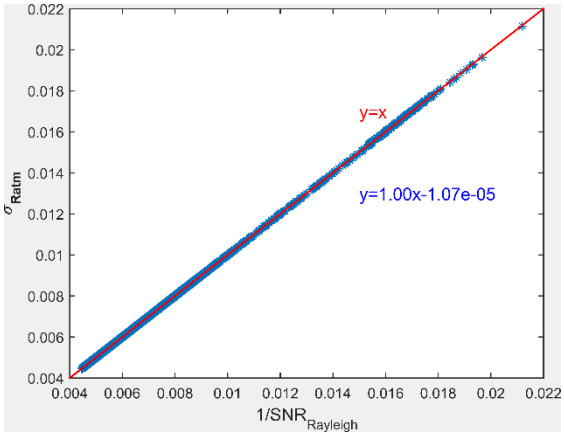

Figure A2. The scatter plot between reciprocal SNR and uncertainty of response function of Rayleigh channel and their first order fitting relationship.

The variables used in the verification of Eq. (A3) can be also used in the verification of Eq. (11). The variable of $\partial v_{HLOS}/\partial R_{ATM}$ is also needed, which is the function of temperature and pressure, and can be obtained through a pre-calculated lookup table. The verification results of Eq. (11) are shown in Fig. A3.

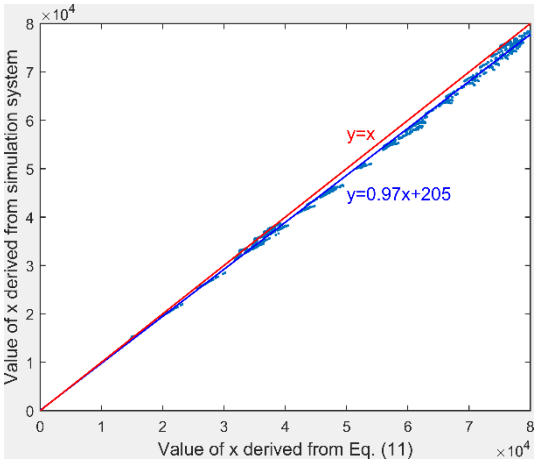

Figure A3. The scatter plot of the values of x which are derived from Eq. (11) and simulation system which is the sum of N_A and N_B respectively.

As is shown in Fig. A3, the fitting line of the scatter plot of value x derived from Eq. (11) and simulation system is very close to the line $y = x$. Furthermore, the residuals between the scattered points and the fitted line are very small, which indicate the wide feasibility of Eq. (11). In addition, it is noteworthy that the scattered points of Fig. A3 are mostly located

below the line $y = x$, which indicates that the value of x calculated by Eq. (11) is smaller than the actual value. According to Sect. 3.3, the laser pulse energy is derived based on the equation $E_{new}/E_{Aeolus} \approx x2/x1$. And $x1$ is obtained from simulation system, which is regarded to be close to real value. The smaller $x2$ may lead to smaller E_{new}, which is about 0.97 times to the real value.

Code and Data availability. The codes in this article are mainly compiled using matlab and are available upon request from the first author by email, zhang01020@hotmail.com. The databases used in this paper include: OMI database, which provided the latitude-averaged temperature, pressure, and ozone, can be accessed via anonymous ftp from toms.gsfc.nasa.gov/ pub/LLM_climatology; LIVAS database, providing the golabl aerosol optical properties with 1°×1° grid, offered by Dr. V. Amiridis from Institude for space applications and remote sensing, National observatory of Athens, and can be assessed from http://lidar.space.no a.gr:8080/livas/; the global LER database is available upon request from the authors, Dr. R. B. A. Koelemeijer from Air Research Laboratory, National Institute of Public Health and the Environment, robert.koelemeijer@rivm.nl; and the reanalysis data of 20th Century Reanalysis provided by the NOAA/OAR/ESRL PSD, Boulder, Colorado, USA, from their Web site at https://www.esrl.noaa.gov/psd/.

Author contributions. CZ, XS, and WL designed the studies; CZ built the simulation systems, performed the computation and analysis, and wrote the paper text; YS, ND, and SL provided important information on data delivery and processing. All authors engaged in discussions on studies, interpretation of results, as well as contribution to the finalization of the paper text.

Competing interests. The authors declare that they have no conflict of interest.

Acknowledgements. Thanks for the helpful discussions provided by Dr. Karsten Schmidt from DLR, Dr. Gert-Jan Marseille and Dr. Ad Stoffelen from Royal Netherlands Meteorological Institute in the building simulation system of Aeolus-type spaceborne DWLs. Thanks for the suggestions provided by Dr. Claudia Emde in running the libRadtran.

Financial support. This research was supported by National Natural Science Foundation of China (NSFC) (41575020).

References:

Amiridis, V., Marinou, E., Tsekeri, A., Wandinger, U., Schwarz, A., Giannakaki, E., Mamouri, R., Kokkalis, P., Binietoglou, I., Solomos, S., Herekakis, T., Kazadzis, S., Gerasopoulos, E., Proestakis, E., Kottas, M., Balis, D., Papayannis, A., Kontoes, C., Kourtidis, K., Papagiannopoulos, N., Mona, L., Pappalardo, G., Le Rille, O. and Ansmann, A.: LIVAS: a 3-

D multi-wavelength aerosol/cloud database based on CALIPSO and EARLINET, Atmos. Chem. Phys., 15(13), 7127-7153, https://doi.org/10.5194/acp-15-7127-2015, 2015.

Baars, H., Geiß, A., Wandinger, U., Herzog, A., Engelmann, R., Bühl, J., Radenz, M., Seifert, P., Althausen, D., Heese, B., Ansmann, A., Martin, A., Leinweber, R., Lehmann, V., Weissmann, M., Cress, A., Filioglou, M., Komppula, M. and Reitebuch, O.: First results from the German CAL/VAL activities for Aeolus, The 29th International Laser Radar Conference, Hefei, China, 2019.

Compo, G. P., Whitaker, J. S., Sardeshmukh, P. D., Matsui, N., Allan, R. J., Yin, X., Gleason, B. E., Vose, R. S., Rutledge, G., Bessemoulin, P., Brönnimann, S., Burnet, M., Crouthamel, R. I., Grant, A. N., Groisman, P. Y., Jones, P. D., Kruk, M. C., Kruger, A. C., Marshall, G. J., Maugeri, M., Mok, H. Y., Nordli, Ø., Ross, T. F., Trigo, R. M., Wang, X. L., Woodruff, S. D. and Worley, S. J.: The Twentieth Century Reanalysis Project, Q. J. Roy. Meteor. Soc., 137(654), 1-28, https://doi.org/10.1002/qj.776, 2011.

Emde, C., Buras-Schnell, R., Kylling, A., Mayer, B., Gasteiger, J., Hamann, U., Kylling, J., Richter, B., Pause, C., Dowling, T. and Bugliaro, L.: The libRadtran software package for radiative transfer calculations (version 2.0.1). Geosci. Model Dev., 9(5), 1647-1672, https://doi.org/10.5194/gmd-9-1647-2016, 2016.

Flesia, C. and Korb, C. L.: Theory of the double-edge molecular technique for Doppler lidar wind measurement, Appl. Opt., 38(3), 432-440, 1999.

Hasinoff, S. W., Durand, F. and Freeman, W. T.: Noise-Optimal Capture for High Dynamic Range Photography, Proceedings of the IEEE Computer Society Conference on Computer Vision and Pattern Recognition, Los Alamitos, 553-560, https://doi.org/10.1109/CVPR.2010.5540167, 2010.

Heliere, A., Bezy, J. L., Bensi, P. and Ingmann, P.: System definition of the ESA Earth Explorer WALES mission, Sensors, Systems, and Next-Generation Satellites VI, Crete, Greece, 24-32, 2002.

Ishii, S., Baron, P., Aoki, M., Mizutani, K., Yasui, M., Ochiai, S., Sato, A., Satoh, Y., Kubota, T., Sakaizawa, D., Oki, R., Okamoto, K., Ishibashi, T., Tanaka, T. Y., Sekiyama, T. T., Maki, T., Yamashita, K., Nishizawa, T., Satoh, M. and Iwasaki, T.: Feasibility study for future space-borne coherent Doppler wind lidar, Part 1: Instrumental Overview for Global Wind Profile Observation, J. Meteorol. Soc. Jpn., 95(5), 301-317, https://doi.org/10.2151/jmsj.2017-017, 2017.

Koelemeijer, R., de Haan, J. F. and Stammes, P.: A database of spectral surface reflectivity in the range 335-772 nm derived from 5.5 years of GOME observations, J. Geophy. Res.-Atmos., 108(D2), 171-181, https://doi.org/10.1029/2002JD002429, 2003.

Liu, Z., Hunt, W., Vaughan, M., Hostetler, C., Mcgill, M., Powell, K., Winker, D. and Hu, Y.: Estimating random errors due to shot noise in backscatter lidar observations, Appl. Opt., 45(18), 4437-4447, https://doi.org/10.1364/AO.45.004437, 2006.

Ma, Z., Riishojgaard, L. P., Masutani, M., Woollen, J. S. and Emmitt, G. D.: Impact of different satellite wind lidar telescope configurations on NCEP GFS forecast skill in observing system simulation experiments, J. Atmos. Ocean. Tech., 32(3), 478-495, https://doi.org/10.1175/JTECH-D-14-00057.1, 2015.

Marseille, G. J. and Stoffelen, A.: Simulation of wind profiles from a space-borne Doppler wind lidar. Q. J. Roy. Meteor. Soc., 129(594A), 3079-3098, https://doi.org/10.1256/003590003769682183, 2003.

Marseille, G., Stoffelen, A. and Barkmeijer, J.: Impact assessment of prospective spaceborne Doppler wind lidar observation scenarios, Tellus A, 60(2), 234-248, https://doi.org/10.1111/j.1600-0870.2007.00289.x, 2008.

Masutani, M., Woollen, J. S., Lord, S. J., Emmitt, G. D., Kleespies, T. J., Wood, S. A., Greco, S., Sun, H. B., Terry, J., Kapoor, V., Treadon, R. and Campana, K. A.: Observing system simulation experiments at the National Centers for Environmental Prediction, J. Geophys. Res.-Atmos., 115(D7), https://doi.org/10.1029/2009JD012528, 2010.

Mcpeters, R., Kroon, M., Labow, G., Brinksma, E., Balis, D., Petropavlovskikh, I., Veefkind, J. P., Bhartia, P. K. and Levelt, P. F.: Validation of the Aura Ozone Monitoring Instrument total column ozone product, J. Geophys. Res.-Atmos., 113 (15). https://doi.org/10.1029/2007JD008802, 2008.

Nakajima, T. Y., Imai, T., Uchino, O. and Nagai, T.: Influence of daylight and noise current on cloud and aerosol observations by spaceborne elastic scattering lidar. Appl. Opt., 38(24), 5218-28, https://doi.org/10.1364/AO.38.005218, 1999.

Paffrath, U.: Performance assessment of the Aeolus Doppler wind lidar prototype, Doctor of Engineering, Ludwig-Maximilians-Universität München, 2006.

Reitebuch, O., Huber, D. and Nikolaus, I.: ADM-Aeolus ATBD Level 1B Product, European Space Agency, 2018.

Rennie, M.: CCN6 results: further Chain-of-Processors testing of L2B results and testing of CCN6 L2B processor algorithm updates, European Centre for Medium-Range Weather Forecasts, 2017.

Stoffelen, A., Marseille, G. J., Bouttier, F., Vasiljevic, D., de Haan, S. and Cardinali, C.: ADM-Aeolus Doppler wind lidar Observing System Simulation Experiment, Q. J. Roy. Meteor. Soc., 132(619B), 1927-1947, https://doi.org/10.1256/qj.05.83, 2006.

Stoffelen, A., Pailleux, J., Kallen, E., Vaughan, J. M., Isaksen, L., Flamant, P., Wergen, W., Andersson, E., Schtberg, H., Culoma, A., Meynart, R., Endemann, M. and Ingmann, P.: The atmospheric dynamics mission for global wind field measurement, B. Am. Meteorol. Soc., 86(1), 73, https://doi.org/10.1175/BAMS-86-1-73, 2005.

Straume, A. G., Rennie, M., Isaksen, L., de Kloe, J., Marseille, G. J., Stoffelen, A., Flament, T., Stieglitz, H., Dabas, A., Huber, D., Reitebuch, O., Lemmerz, C., Lux, O., Marksteiner, U., Weiler, F., Witschas, B., Meringer, M., Schmidt, K., Nikolaus, I., Geiss, A., Flamant, P., Kanitz, T., Wernham, D., von Bismarck, J., Bley, S., Fehr, T., Floberghagen, R. and Parrinello, T.: ESA's space-based Doppler wind lidar mission Aeolus first wind and aerosol product assessment results, The 29th International Laser Radar Conference, Hefei, China, 2019.

Sun, X. J., Zhang, R. W., Marseille, G. J., Stoffelen, A., Donovan, D., Liu, L. and Zhao, J.: The performance of Aeolus in heterogeneous atmospheric conditions using high-resolution radiosonde data, Atmos. Meas. Tech., 7(8), 2695-2717. https://doi.org/10.5194/amt-7-2695-2014, 2014.

Tan, D. G. H., Anderson, E., De Kloe, J., Marseille, G., Stoffelen, A., Poli, P., Denneulin, M., Dabas, A., Huber, D., Reitebuch, O., Flamant, P., Le Rille, O. and Nett, H.: The ADM-Aeolus wind retrieval algorithms, Tellus A, 60(2), 191-205. https://doi.org/10.1111/j.1600-0870.2007.00285.x, 2008.

Vahlbruch, H., Mehmet, M., Chelkowski, S., Hage, B., Franzen, A., Lastzka, N., Gossler, S., Danzmann, K. and Schnabel, R.: Observation of squeezed light with 10-dB quantum-noise reduction, Phys. Rev. Lett., 100(3), 033602, https://doi.org/10.1103/PhysRevLett.100.033602, 2008.

Zhang, C. L., Sun, X. J., Zhang, R. W. and Liu, Y. W.: Simulation and assessment of solar background noise for spaceborne lidar, Appl. Opt., 57(31), 9471-9479, https://doi.org/10.1364/AO.57.009471, 2018.

Zhang, C. L., Sun, X. J., Zhang, R. W., Zhao, S. J., Lu, W., Liu, Y. W. and Fan, Z. Q.: Impact of solar background radiation on the accuracy of wind observations of spaceborne Doppler wind lidars based on their orbits and optical parameters, Opt. Express, 27(12), A936-A952, https://doi.org/10.1364/OE.27.00A936, 2019.

Zhang, R. W., Sun, X. J., Yan, W., Zhao, J., Liu, L., Li, Y., Zhang, C. L. and Zhou, J. H.: Simulation of frequency discrimination for spaceborne Doppler wind lidar (II): Study on the retrieval of atmospheric wind speed for Rayleigh channel based on Fabry-Perot interferometer, Acta Phys. Sin.-Ch. Ed., 63(14), 147-156. https://doi.org/10.7498/aps.63.140703, 2014.